metals

MDPI

Article

Thermodynamic and Experimental Investigation of Lead Removal from Pb-Sb Alloy Using an H_3PO_4-$(NaPO_3)_6$ Composite Agent

Jiahui Tan [1,2], Xiangfeng Kong [1,2], Jia Yang [1,2], Dachun Liu [1,2] and Hongwei Yang [1,2,*]

[1] Faculty of Metallurgical and Energy Engineering, Kunming University of Science and Technology, Kunming 650093, China
[2] National Engineering Research Center of Vacuum Metallurgy, Kunming University of Science and Technology, Kunming 650093, China
* Correspondence: hongweiy@kust.edu.cn; Tel.: +86-139-8715-7570

Abstract

This study presents a rapid and efficient laboratory-scale process for removing lead from Pb–Sb alloy melts using a composite H_3PO_4–$(NaPO_3)_6$ flux. Thermodynamic analysis was combined with experimental investigation to elucidate the influence of key parameters on lead removal behavior. The Wilson equation was employed to describe the non-ideal behavior of the Pb–Sb system, enabling estimation of equilibrium lead contents and providing theoretical support for interpreting experimental trends. Under the investigated conditions (1073 K, H_3PO_4/$(NaPO_3)_6$ mass ratio of 2:1, and a holding time of 10 min), the Pb mass fraction was reduced from 10.0 wt.% to 0.018 wt.%, corresponding to a lead removal efficiency of 99.86%. Compared with the traditional refining processes, this method shortens the processing time and avoids the use of volatile gas reagents, demonstrating its potential for lead–antimony separation. The results provide thermodynamic and experimental insight into phosphate-based refining of crude antimony.

Keywords: antimony pyrometallurgy; lead removal agent; polyphosphate; Wilson equation; phosphates; activity coefficients

1. Introduction

Antimony is a critical strategic metal widely used in flame retardants, high-performance alloys, and semiconductor devices—applications that demand strict control of heavy-metal impurities [1–4]. Antimony and lead resources face declining reserves, lower grades, and complex occurrence states; the two metals frequently coexist (e.g., jamesonite contains ca. 28–32 wt.% Pb and 24–28 wt.% Sb [5]). This association, together with secondary Pb–Sb alloys generated during industrial applications, inevitably produces substantial amounts of Pb–Sb alloys in smelting and recycling. Without further processing, these alloys both waste strategic resources and pose environmental risks due to heavy-metal leakage, making their efficient treatment an urgent metallurgical need.

Among these Pb–Sb-containing intermediates, crude antimony is a typical feed where Pb removal is particularly challenging. During the mining and smelting of antimony ores, lead is inevitably introduced into crude antimony (typically 5–15 wt.% [6]), and its separation remains a bottleneck for high-value utilization of antimony resources. This difficulty arises from the similar physicochemical properties of Pb and Sb, e.g., comparable melting points and mutual solubility in melts [6], which hinder efficient purification.

Check for updates

Academic Editor: Antoni Roca

Received: 26 December 2025
Revised: 20 January 2026
Accepted: 21 January 2026
Published: 23 January 2026

Copyright: © 2026 by the authors. Licensee MDPI, Basel, Switzerland. This article is an open access article distributed under the terms and conditions of the Creative Commons Attribution (CC BY) license.

To address this challenge, various approaches have been explored for Pb removal from crude antimony. Although vacuum distillation is effective for processing complex metallurgical feeds and recovering secondary resources [7–15], its application to the Pb–Sb system is constrained by azeotropic behavior, which limits separation based on volatility differences [16]. Consequently, chemical refining is often required, making the choice of an appropriate lead removal agent critical.

Among the various lead removal agents used in chemical refining, phosphate-based reagents have been widely investigated in both industrial and laboratory settings. Conventional agents such as orthophosphoric acid often suffer from long reaction times and considerable antimony losses [17,18]. To improve performance, Liu et al. [19] developed a liquid reagent based on phosphoric acid derivatives and sodium phosphate; however, the process relied on nitrogen atomization and auxiliary equipment, complicating simplification and industrial implementation. Ye et al. [20,21] employed $NaPO_3$ as a lead removal agent and effectively decreased the lead content in crude antimony; however, their thermodynamic analysis assumed an ideal solution, neglecting the non-ideal behavior of Pb–Sb melts and causing deviations in equilibrium predictions. Zhang et al. [22] prepared a composite reagent consisting of phosphoric acid derivatives and sodium polyphosphate, achieving satisfactory lead removal but without systematic optimization of key operating parameters. More recently, Zhang et al. [23] proposed a molten-salt route using Sb_2O_3, P_2O_5, H_2O, Sb_2S_3, and K/Na salts, reducing the lead content to 0.03% without harmful gas emissions; however, the resulting slag contained pungent and unstable metabisulfites that may decompose to SO_2 at high temperatures, posing potential environmental risks.

Therefore, this study proposes a chemical refining method using an H_3PO_4-$(NaPO_3)_6$ composite reagent. Phosphate reagents can react with lead to form chemically stabilized Pb-containing species [12–14], while polyphosphates (e.g., $(NaPO_3)_6$) may promote interfacial reactions and mass transfer in the molten phase. This work aims to investigate a rapid and low-emission laboratory-scale lead removal process for crude antimony (a Pb–Sb alloy) and to clarify the role of thermodynamic analysis in interpreting lead removal behavior, rather than to establish optimized industrial operating conditions.

2. Materials and Methods

2.1. Experimental Procedure

Crude antimony was treated as a Pb–Sb binary alloy for sample preparation. High-purity antimony particles (≥99.99%) were crushed to 5–10 mm and mixed with high-purity lead particles (≥99.99%) at a mass ratio of 9:1 in a graphite crucible. The mixture was melted at 1073 K for 20 min in a pit-type electric resistance furnace under argon. To ensure homogeneity, the melt was stirred, turned over, remelted, and then cooled to obtain the final sample.

The composite lead removal agent consisted of H_3PO_4 solution and $(NaPO_3)_6$. Before each experiment, the components were weighed according to the specified mass ratio, thoroughly premixed, and added into the crucible. Lead removal experiments were conducted under varying process parameters, including temperature, reagent ratio $H_3PO_4/(NaPO_3)_6$, and reaction time.

For each run, 10.0 g of the Pb–Sb alloy was charged into a graphite crucible together with the premixed composite reagent. The crucible was placed in a vertical tube furnace under flowing argon and heated at 8 $K \cdot min^{-1}$ to the target temperature, then held for the prescribed reaction time. After the reaction, power was cut, the crucible was withdrawn, and the sample was allowed to cool to room temperature.

After cooling, the metal and slag phases were separated mechanically. Residual surface slag adhering to the antimony phase was removed; both phases were ground

to <75 μm for chemical analysis. Pb and Sb were quantified by ICP-OES (6300, Thermo Electron Corporation, Waltham, MA, USA) after acid digestion. The experimental flow chart is shown in Figure 1. Considering the laboratory-scale setup, the main sources of experimental uncertainty include temperature fluctuation (±10 °C), mass measurement (±0.01 g), and chemical analysis by ICP-OES. The reported results emphasize comparative trends obtained under identical experimental procedures.

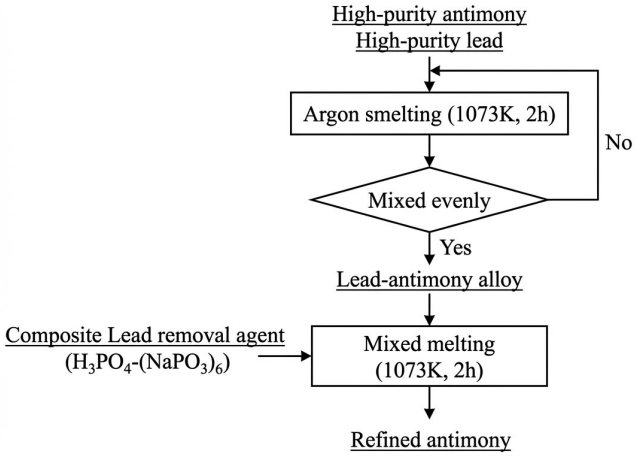


Figure 1. Experimental flowchart.

2.2. Calculation of Lead Removal Efficiency

The lead removal efficiency (η_{Pb}) was calculated based on the total lead mass in the Sb–Pb system before and after the process, using the following equations:

$$[\mathrm{Pb}]_{\mathrm{initial}} = \mathrm{m}_1 \cdot [\mathrm{Pb}\%]_{\mathrm{initial}} \quad (1)$$

$$[\mathrm{Pb}]_{\mathrm{final}} = \mathrm{m}_2 \cdot [\mathrm{Pb}\%]_{\mathrm{final}} \quad (2)$$

$$\eta_{Pb} = \frac{[Pb]_{initial} - [Pb]_{final}}{[Pb]_{initial}} \cdot 100\% \quad (3)$$

where η_{Pb} = lead removal efficiency from crude antimony. $[\mathrm{Pb}]_{\mathrm{initial}}$ and $[\mathrm{Pb}]_{\mathrm{final}}$ are the total masses (g) in the sample before and after smelting, respectively; m_1 and m_2 are the corresponding sample masses (g).

3. Theoretical Basis

3.1. Thermodynamic Calculation

The lead removal mechanism of the composite reagent is described by the reactions below. Standard thermodynamic data for the involved species are summarized in Tables 1 and 2 [24]. In all expressions, T is in K and ΔG° is in kJ/mol, all thermodynamic data and reaction Gibbs free energies refer to pure substances in their stable phases at atmospheric pressure and temperature.

$$2\mathrm{Pb} + \mathrm{O_2} = 2\mathrm{PbO},\ \Delta G^\circ = -434.6 + 0.1684\mathrm{T}\ (\mathrm{kJ/mol}) \quad (4)$$

$$4\mathrm{Sb} + 3\mathrm{O_2} = 2\mathrm{Sb_2O_3},\ \Delta G^\circ = -1410.8 + 0.4964\mathrm{T}\ (\mathrm{kJ/mol}) \quad (5)$$

$$\mathrm{Sb_2O_3} + 3\mathrm{Pb} = 3\mathrm{PbO} + 2\mathrm{Sb},\ \Delta G^\circ = 53.5 - 0.0224\mathrm{T}\ (\mathrm{kJ/mol}) \quad (6)$$

$$3\mathrm{PbO} + \mathrm{P_2O_5} = \mathrm{Pb_3(PO_4)_2},\ \Delta G^\circ = -210 + 0.0671\mathrm{T}\ (\mathrm{kJ/mol}) \quad (7)$$

$$2\mathrm{H_3PO_4} + 3\mathrm{PbO} = \mathrm{Pb_3(PO_4)_2} + 3\mathrm{H_2O},\ \Delta G^\circ = 238.7 - 0.0559\mathrm{T}\ (\mathrm{kJ/mol}) \quad (8)$$

$$6Pb + 3O_2 + 4H_3PO_4 = 2Pb_3(PO_4)_2 + 6H_2O,\ \Delta G^\circ = -411.98 + 0.1112T\ (kJ/mol) \quad (9)$$

Table 1. Standard molar enthalpy and standard molar entropy of substances in lead removal reactions.

Substance	PbO	H_2O (g)	P_2O_5	$Pb_3(PO_4)_2$	Sb_2O_3	H_3PO_4 (L)
ΔH^θ (kJ/mol)	−217.32	−241.82	−1505.40	−1898.00	−708.24	−1288.34
ΔS^θ J/(mol·K)	68.70	188.83	228.90	206.60	125.10	150.80

Table 2. Melting points of substances.

Substance	PbO	P_2O_5	$Pb_3(PO_4)_2$	Sb_2O_3	Pb	Sb
Melting point (K)	1159	853	1287	928	600	903

The lead removal effect is achieved through the synergistic reaction of the composite agent components with lead, forming stable lead phosphate. Figure 2 presents the Gibbs free energy (ΔG) as a function of temperature for these reactions. Within the temperature range of 873–1073 K, most key reactions involved in lead removal exhibit negative ΔG values, indicating their thermodynamic feasibility under the experimental conditions. Although Equation (6) shows slightly positive ΔG values, it is not the dominant pathway for lead removal in the present composite reagent system.

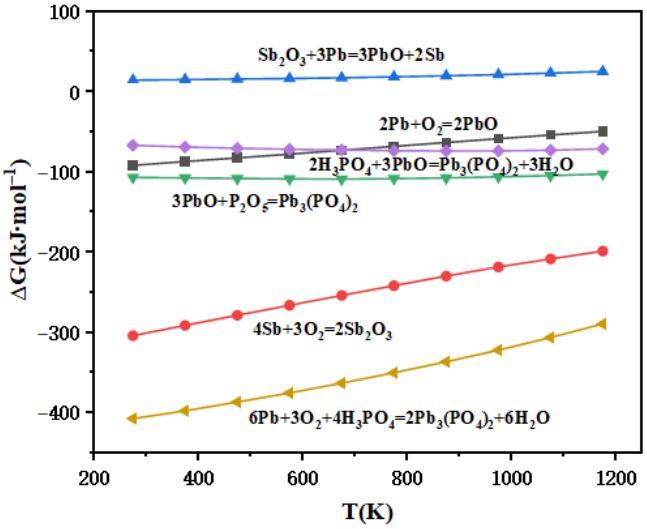


Figure 2. Gibbs free energy versus temperature for each reaction process.

Within 873–1073 K, most reactions exhibit negative ΔG° values (Figure 2), indicating that lead is readily converted to PbO and further to stable $Pb_3(PO_4)_2$ under the oxygen potential supplied by P_2O_5/H_3PO_4. Table 2 shows that Pb and Sb are molten in this range, while P_2O_5 is liquid, which enhances mass transfer and reaction contact.

Although H_3PO_4 alone can remove lead, it often results in antimony losses and encapsulation of antimony droplets by viscous slag, as reported in previous studies [20]. In the composite system, H_3PO_4 decomposes below ~973 K to release P_2O_5 that preferentially reacts with PbO to form $Pb_3(PO_4)_2$. Sodium polyphosphate $(NaPO_3)_6$ decomposes at higher temperatures (>973 K), replenishing P_2O_5 and sustaining the reaction rate in the mid-to-late stages. Its decomposition product Na_2O forms low-melting mixtures with Sb_2O_3, reducing slag viscosity, improving flowability, and thereby mitigating mechanical entrapment of antimony droplets. A schematic of the overall mechanism is shown in Figure 3.

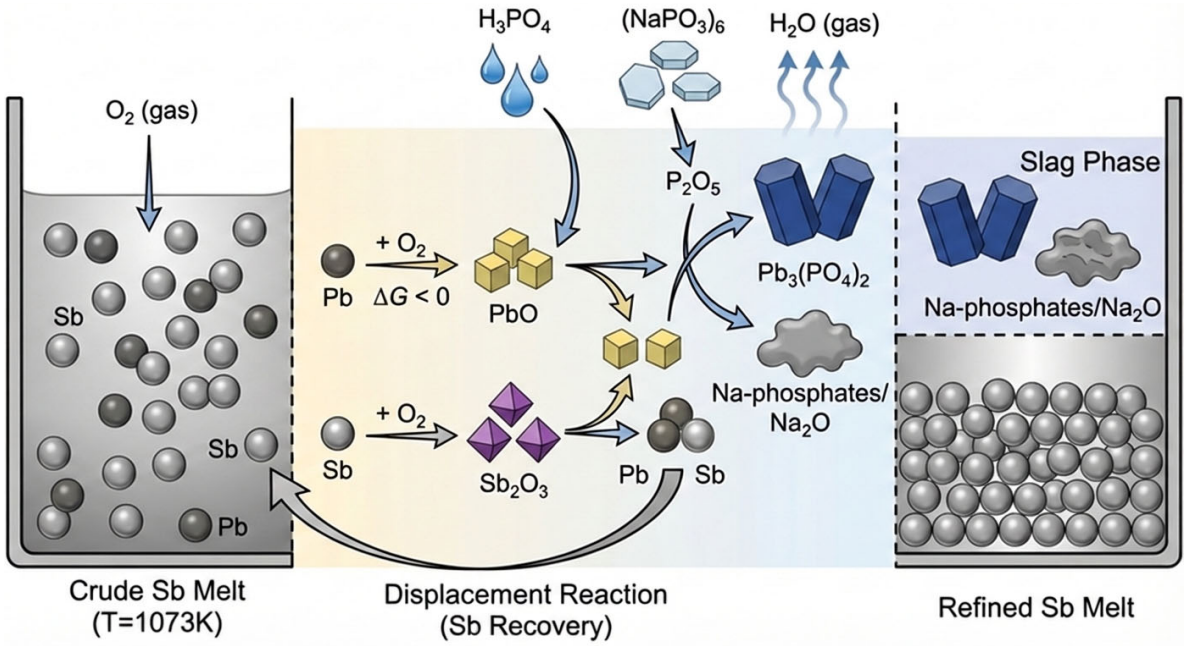


Figure 3. Schematic diagram of reaction mechanism in the lead removal process.

As illustrated in Figure 3, during the lead removal process, Pb and Sb react with O_2 to form PbO and Sb_2O_3. The resulting Sb_2O_3 forms a solid slag layer on the surface of the molten mixture, preventing oxygen from contacting the internal antimony and thus inhibiting its further oxidation.

3.2. Activity of Components for the Pb-Sb Binary System

The ideal solution model neglects interactions between Pb and Sb atoms, leading to inaccurate predictions of reaction equilibria in Pb–Sb melts. To correct for this non-ideal behavior, the activity coefficients of Pb and Sb were calculated using the Wilson equation [25], which is based on local composition theory. For a binary (i–j) liquid alloy, the excess Gibbs free energy (G^E) of the Wilson equation is given by:

$$\frac{G^E}{RT} = -x_i ln(x_i + A_{ij}x_j) - x_j ln(x_j + A_{ji}x_i) \tag{10}$$

where G^E is excess Gibbs free energy; x_i and x_j are molar fractions of components i and j, respectively; R is ideal gas constant; T is system temperature; A_{ij}, A_{ji} are Wilson equation parameters, defined as:

$$A_{ij} = \frac{v_j}{v_i} exp\left[-\frac{(\lambda_{ij} - \lambda_{ii})}{RT}\right] \tag{11}$$

$$A_{ji} = \frac{v_i}{v_j} exp\left[-\frac{(\lambda_{ji} - \lambda_{jj})}{RT}\right] \tag{12}$$

where v_i and v_j are molar volumes of components i and j (temperature-dependent), respectively; λ_{ii}, λ_{ij}, λ_{jj} are atomic pair interaction energies for i–i, i–j, and j–j pairs (assumed to be temperature-independent), respectively [26].

Differentiating Equation (7) with respect to x_i (or x_j) yields the activity coefficient equations for components i and j:

$$ln\gamma_i = -ln(x_i + A_{ij}x_j) + x_j\left(\frac{A_{ij}}{x_i + A_{ij}x_j} - \frac{A_{ji}}{x_j + A_{ji}x_i}\right) \tag{13}$$

$$ln\gamma_j = -ln(x_j + A_{ji}x_i) - x_i\left(\frac{A_{ij}}{x_i + A_{ij}x_j} - \frac{A_{ji}}{x_j + A_{ji}x_i}\right) \quad (14)$$

By substituting the experimental values of the activity coefficients of the components into Equations (13) and (14), and parameters A_{ij} and A_{ji} of the Wilson equation can be obtained. The relevant temperature correlation formulas are presented in Equations (15) and (16):

$$A'_{ij} = \frac{v'_j}{v'_i}\left(\frac{A_{ij}v_i}{v_j}\right)^{\frac{T}{T'}} \quad (15)$$

$$A'_{ji} = \frac{v'_i}{v'_j}\left(\frac{A_{ji}v_j}{v_i}\right)^{\frac{T}{T'}} \quad (16)$$

The Wilson equation parameters A_{ij} and A_{ji} calculated at the experimental temperature T can be used to compute the Wilson equation parameters A'_{ij} and A'_{ji} at different temperatures T′ via temperature correlation formulas. Substituting the temperature-dependent coefficients A'_{ij} and A'_{ji} into Equations (13) and (14) provides the corresponding activity coefficients for the alloy components. Experimental activity coefficients of binary liquid alloy components were retrieved from the literature [27], and relevant parameters were sourced from [28]. Wilson equation parameters A_{ij} and A_{ji} at the experimental temperature were obtained by substituting experimental activity coefficients into Equations (13) and (14). Table 3 lists these parameters for the Pb-Sb system, and Table 4 provides molar volume formulas for relevant metals. Comparison of calculated activity values and experimental data [26] for the Pb-Sb binary system at 905 K is presented in Table 5 (The average absolute error (AAE) between calculated and experimental values is 0.02, with a correlation coefficient R^2 of 0.99) and Figure 4.

Table 3. Wilson equation parameters for the Pb-Sb system.

$i-j$	T/K	A_{ij}	A_{ji}
Sb-Pb	905	1.2838	1.3022

Table 4. Formulas for the molar volume of Sb and Pb, Adapted from Ref. [28].

Element	v (cm^3/mol)	T/K
Sb	$18.8\,[1 + 1.3 \times 10^{-4}\,(T - 904)]$	904–1860
Pb	$19.42\,[1 + 1.24 \times 10^{-4}\,(T - 600)]$	600–2022

Table 5. Comparison of calculated activities and experimental date, Adapted from Ref. [27] for the Pb-Sb system at 905 K.

x_{Pb}	$a_{Pb,Exp.}$	$a_{Sb,Exp.}$	$a_{Pb,Cal.}$	$a_{Sb,Cal.}$
0.1	0.078	0.897	0.064	0.895
0.2	0.164	0.789	0.141	0.782
0.3	0.261	0.678	0.230	0.666
0.4	0.365	0.566	0.329	0.549
0.5	0.474	0.457	0.436	0.436
0.6	0.584	0.354	0.550	0.329
0.7	0.693	0.257	0.666	0.230
0.8	0.799	0.167	0.783	0.141
0.9	0.900	0.083	0.895	0.064

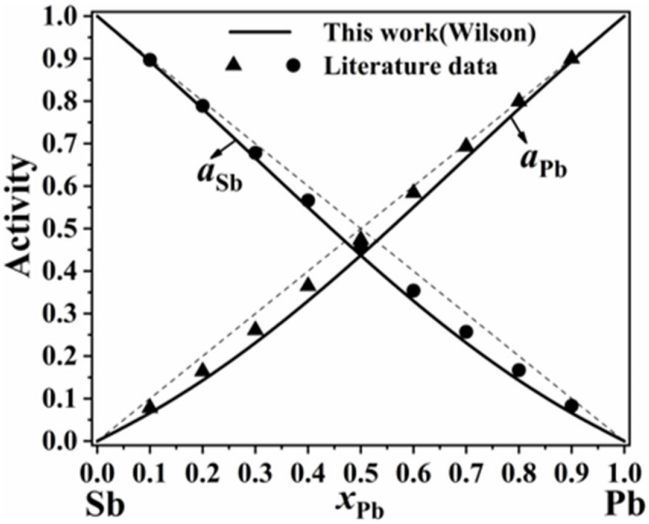


Figure 4. Comparison of calculated activities (lines) and experimental data (points) for the Pb-Sb binary system at 905 K.

4. Results and Discussion

4.1. Thermodynamic Estimation of Residual Lead Content

The initial Pb mass fraction in the Pb–Sb alloy was 10.0 wt.%, corresponding to a molar fraction of x_{Pb} = 0.0612. Using the Wilson parameters (Tables 3 and 4), the activity coefficients of lead, γ_{Pb}, were calculated. With the activity definition $a_{Pb} = \gamma_{Pb} x_{Pb}$, the Gibbs free energy change in the core reaction (Equation (6)) was evaluated to estimate the thermodynamic tendency of the core reaction. The resulting equilibrium activities were then converted to corresponding residual lead mass fractions for comparison purposes (Table 6).

Table 6. Predicted equilibrium residual Pb mass fraction as a function of temperature for an initial 10.0 wt.% Pb alloy.

Temperature (K)	wt.% Pb
973	0.0602
1023	0.0607
1073	0.0610
1123	0.0614
1173	0.0617

As shown in Table 6, the thermodynamically estimated residual Pb mass fraction shows a slight increasing trend with temperature (973–1173 K). This trend is thermodynamically reasonable: increasing temperature makes (ΔG^0) less negative, reduces the equilibrium constant, and thus raises the equilibrium Pb content in the metal phase. Notably, the initial a_{Pb} is much higher than the equilibrium a_{Pb}, indicating a strong driving force for Pb removal under the studied conditions. The deviation of γ_{Pb} from unity further confirms the pronounced non-ideal behavior of the Pb–Sb melt and highlights the need for activity corrections when making equilibrium predictions. It should be noted that the calculated values represent thermodynamic tendencies rather than the actual experimental residual lead contents, as kinetic factors and interfacial mass transfer also play important roles under the present laboratory conditions.

Regarding the phase constitution of the final slag, lead is inferred to be incorporated into a complex phosphate–oxide network rather than forming a single crystalline phase. Due to the multi-component nature of the slag and the rapid cooling rates post-experiment, the formation of well-defined crystalline lead phosphates is often suppressed. Consequently,

the removal mechanism is substantiated by the high elemental removal efficiency and thermodynamic feasibility, even if specific crystalline diffraction peaks are not prominent.

4.2. Effect of Lead Removal Agent Mass Ratio

With the total addition of the composite agent fixed at 30% of the alloy mass, a reaction temperature of 1073 K, and a holding time of 10 min, the effect of the $H_3PO_4/(NaPO_3)_6$ mass ratio was investigated (Table 7 and Figure 5).

Table 7. Effect of $H_3PO_4/(NaPO_3)_6$ mass ratio on lead removal.

$m(H_3PO_4)/m((NaPO_3)_6)$	Lead Content (%)	Antimony Direct Recovery Rate (%)	Lead Removal Efficiency (%)
1/1	0.640	91.2	94.16
1.5/1	0.052	86.9	99.55
2/1	0.034	89.1	99.69
1/1.5	1.420	92.0	87.00
1/2	3.500	92.9	68.00

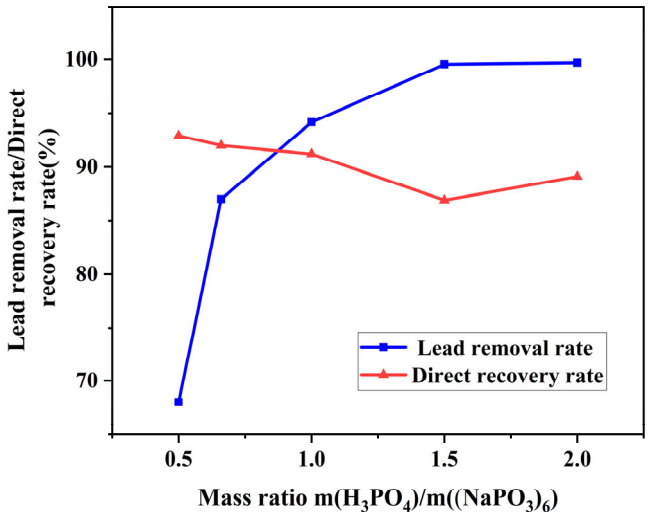


Figure 5. Experimental results for different ratios of lead removal agent.

When the ratio increased from 1:1 to 2:1, the lead removal efficiency improved markedly from 94.16% to 99.69%, while the direct Sb recovery also increased overall and reached 89.1% at 2:1. This behavior is attributed to a synergistic effect: H_3PO_4 supplies active phosphate species in the early stage to rapidly immobilize lead as $Pb_3(PO_4)_2$, whereas $(NaPO_3)_6$ sustains phosphate availability and lowers slag viscosity via Na-containing phosphates, mitigating mechanical entrainment of Sb. At too low an H_3PO_4 fraction, the early phosphate supply is insufficient, resulting in incomplete Pb fixation. Conversely, an excessive H_3PO_4 fraction may generate surplus P_2O_5 that reacts with Sb_2O_3, increasing Sb loss. Accordingly, a mass ratio of 2:1 was selected for subsequent experiments, considering both lead removal efficiency and antimony recovery.

4.3. Effect of Lead Removal Agent Addition Amount

At a fixed mass ratio of 2:1, a reaction temperature of 1073 K, and a holding time of 10 min, the effect of the lead removal agent addition on the lead removal behavior was investigated. The addition amount is expressed as wt.% of the alloy to facilitate comparison and discussion.

As shown in Table 8 and Figure 6, increasing the addition from 20 to 60 wt.% of the alloy significantly enhanced the lead removal efficiency, which increased from 97.97%

to 99.84%. At relatively low addition levels (≤30 wt.%), the contact between the lead removal agent and the molten alloy was insufficient, resulting in incomplete reaction and lower lead removal efficiency. In addition, the direct recovery rate of antimony (R_{Sb}) decreased slightly due to volatilization and oxidation losses during the treatment. When the addition reached 50–60 wt.% of the alloy, the lead removal efficiency exceeded 99.8%, and R_{Sb} stabilized above 88%, indicating that the lead removal reaction was nearly complete. Further increasing the addition within this range only marginally improved the lead removal efficiency, while increasing reagent consumption. Considering both the high economic value of antimony and reagent utilization, an addition range of 50–60 wt.% of the alloy was identified as optimal. Therefore, an addition of 60 wt.% of the alloy was selected for subsequent experiments.

Table 8. Effect of lead removal agent addition (20–60 wt.% of alloy) on lead content, antimony direct recovery rate, and lead removal efficiency at 1073 K for 10 min and a mass ratio of 2:1.

Lead Removal Agent Addition (wt.% of Alloy)	Lead Content in Antimony After Removal (%)	Antimony Direct Recovery Rate (%)	Lead Removal Efficiency (%)
20	0.340	89.40	97.97
30	0.210	86.21	98.28
40	0.180	82.90	98.51
50	0.034	88.23	99.41
60	0.018	91.20	99.84

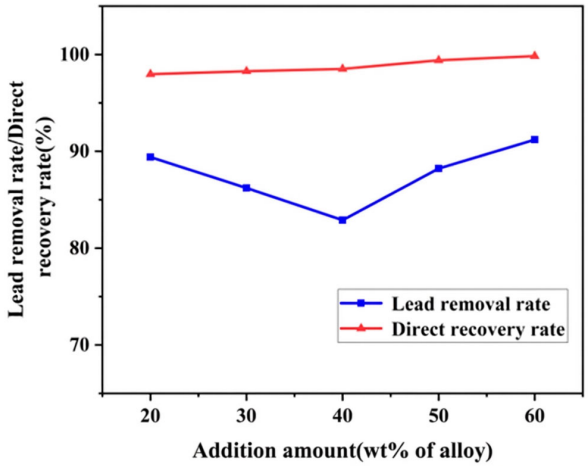


Figure 6. Experimental results for different lead removal agent addition amounts.

It is worth noting that the reagent-to-metal ratio used in this laboratory-scale study is primarily related to the reaction characteristics of lead removal under static conditions. Under laboratory-scale conditions, mass transfer and melt convection are limited compared with industrial furnaces. Therefore, an excess amount of the reagent is required to ensure sufficient contact between Pb and phosphate-related species. In industrial operations, where dynamic mixing and heat transfer conditions are more favorable, reagent consumption could be significantly reduced.

4.4. Effect of Reaction Temperature

Using the optimal mass ratio of 2:1, a composite agent addition amount of 6 g per 10 g of alloy, and a reaction time of 10 min, the influence of temperature was investigated (Table 9 and Figure 7).

Table 9. Effect of reaction temperature on lead removal and direct Sb recovery at a 2:1 mass ratio, 6 g per 10 g alloy, and 10 min.

Temperature (K)	Lead Content in Antimony After Removal (%)	Antimony Direct Recovery Rate (%)	Lead Removal Efficiency (%)
973	0.044	74.0	99.68
1023	0.017	72.0	99.88
1073	0.016	74.5	99.89
1123	0.020	68.5	99.87
1173	0.021	73.2	99.85

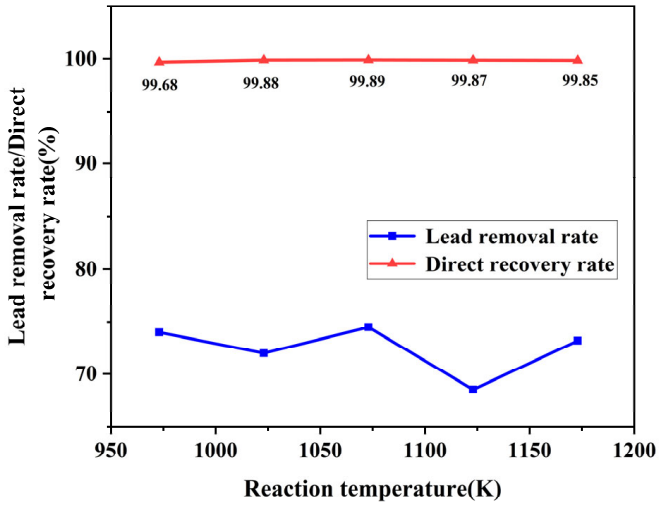


Figure 7. Experimental results at different temperatures.

In the range of 973–1073 K, η_{Pb} increased slightly from 99.68% to 99.89%, consistent with an increased reaction rate. Above 1073 K, η_{Pb} became essentially stable, indicating that the process approached equilibrium under the given addition and time. The direct Sb recovery peaked at 1073 K (74.5%). At lower temperatures (e.g., 1023 K), higher melt/slag viscosity likely hinders mass transfer and promotes entrainment-related losses. At higher temperatures (e.g., 1123 K), Sb volatilization and oxidation become more significant, reducing R_{Sb}. Therefore, 1073 K was selected as a representative reaction temperature for subsequent tests, balancing high η_{Pb} with acceptable R_{Sb}. This temperature also maintains both the phosphate phase and the metal melt fully molten, favoring interfacial contact and reaction.

Regarding the selectivity between Pb and Sb at high temperatures, although antimony constitutes the major metallic phase with high activity, the process exhibits high Pb removal selectivity. This is primarily attributed to the significantly stronger chemical affinity of lead toward phosphate compared to antimony. Furthermore, as a surface-active element, lead tends to enrich at the interface, reacting preferentially with the flux before significant antimony oxidation occurs.

4.5. Effect of Holding Time

At a 2:1 mass ratio, a total addition of 6 g per 10 g alloy, and 1073 K, the influence of holding time was assessed (Table 10 and Figure 8).

Table 10. Effect of holding time on residual Pb, η_{Pb} , and R_{Sb} at 1073 K with a 2:1 mass ratio and 6 g per 10 g alloy.

Holding Time (min)	Lead Content in Antimony After Removal (%)	Antimony Direct Recovery Rate (%)	Lead Removal Efficiency (%)
5	0.019	71.3	99.87
10	0.018	78.7	99.86
15	0.020	76.0	99.85
20	0.019	67.4	99.88

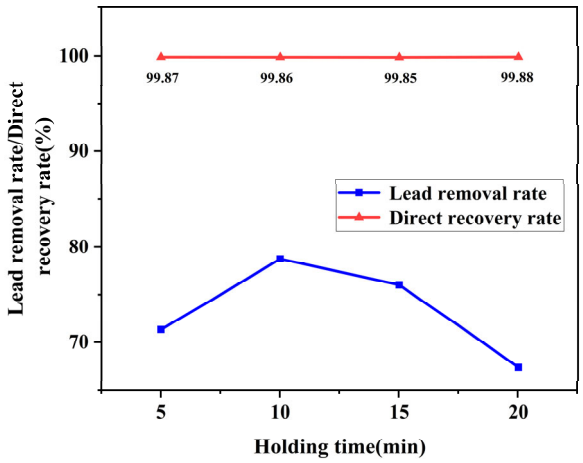


Figure 8. Experimental results for different holding times.

From 5 to 10 min, the residual Pb decreased slightly (0.019% → 0.018%), while R_{Sb} increased from 71.3% to 78.7%, indicating that the interfacial reaction between active phosphate species and dissolved Pb dominated during this period. After 10 min, η_{Pb} remained essentially constant whereas R_{Sb} declined, suggesting that extended holding increases Sb volatilization/oxidation and/or entrainment losses without improving Pb removal. These suggest that Sb losses may be mitigated by limiting the high-temperature residence time and promoting rapid phase separation once lead fixation is achieved. A slight rise in residual Pb at 20 min (to 0.020%) may reflect redistribution of Pb between phases or coarsening/settling effects rather than true phosphate decomposition at 1073 K. Consequently, a holding time of 10 min was adopted for subsequent experiments, considering both performance and energy consumption.

These suggest that Sb losses may be mitigated by limiting the high-temperature residence time and promoting rapid phase separation once lead fixation is achieved.

The non-monotonic variation of antimony recovery (R_{Sb}) with holding time reflects competitive reactions. The initial increase in recovery corresponds to the rapid separation of the lead-rich phase. However, with prolonged holding at elevated temperatures, secondary effects such as mechanical entrainment of metallic antimony droplets into the viscous slag and partial oxidation of antimony become more pronounced, leading to the observed decrease in recovery.

4.6. Kinetics Analysis

To gain insight into the temperature-dependent behavior and the rate-controlling characteristics of lead removal, a kinetic-related analysis was performed based on the core reaction (Equation (6)). The equilibrium constant K at different temperatures was calculated from the thermodynamic relationship $\Delta G = -RTlnK$.

It should be emphasized that the equilibrium constant K can qualitatively reflect the temperature sensitivity of the forward lead fixation process. Consequently, lnK is employed here as an apparent kinetic descriptor, rather than a rigorous rate constant, to analyze the temperature dependence of the process using an Arrhenius-type formalism:

$$lnK = -\frac{E_a}{R} \cdot \frac{1}{T} + lnA \tag{17}$$

(1) Apparent activation energy determination

Linear fitting of lnK versus $\frac{1}{T}$ yields a straight line with a high correlation coefficient ($R^2 > 0.99$) (Figure 9), indicating a clear Arrhenius-type relationship within the investigated temperature range. The slope of the fitted line is approximately $m \approx -12,600$ K. Based on $m = -\frac{E_a}{R}$, the apparent activation energy is calculated to be 105 kJ/mol.

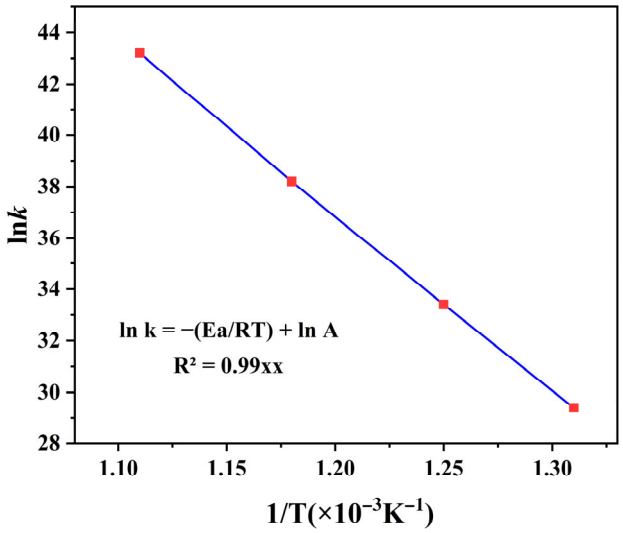


Figure 9. Arrhenius-type plot of ln K versus 1/T for the lead removal process.

This value falls within the typical range reported for chemically controlled interfacial reactions (80–150 kJ/mol), suggesting that interfacial chemical reactions play a dominant role under the present experimental conditions rather than by pure diffusion control, which typically exhibits much lower activation energies.

(2) Temperature-dependent reaction tendency

Within the temperature range of 973–1073 K, the Arrhenius term $\exp\left(-\frac{E_a}{RT}\right)$ increases significantly from 2.5×10^{-6} to 8.3×10^{-6}, indicating an enhanced apparent tendency for lead fixation with increasing temperature. This trend is consistent with the experimentally observed improvement in lead removal efficiency.

When the temperature exceeds 1073 K, the absolute value of the negative Gibbs free energy change decreases, and the system gradually approaches thermodynamic equilibrium. As a result, further increases in temperature provide diminishing driving force, leading to a plateau in lead removal efficiency.

Regarding the holding-time effect (Figure 8), effective contact between active phosphate species (originating from P_2O_5-related species in the slag/melt) and the molten phase promotes rapid lead fixation at the early stage. With prolonged holding at elevated temperatures, phase re-equilibration becomes more pronounced, which may cause a slight rebound in the residual lead content.

Although a rigorous kinetic model is limited by the batch nature of the experiments, the rapid attainment of low residual lead levels suggests that the process is likely controlled by a mix of interfacial chemical reaction and mass transfer through the slag layer. The

slight fluctuation in residual Pb content at longer times suggests the system approaches a quasi-equilibrium state, where minor redistribution or mechanical effects may occur.

5. Conclusions

This study developed an efficient and environmentally friendly process for removing lead from crude antimony using an H_3PO_4–$(NaPO_3)_6$ composite agent. The main conclusions are:

Synergistic action is evident: H_3PO_4 decomposes at low temperature to release reactive phosphate species and rapidly immobilize Pb, while $(NaPO_3)_6$ sustains phosphate supply at higher temperatures and improves melt handling, helping to reduce antimony loss.

Thermodynamic calculations confirmed the spontaneity of all key reactions within the 873–1073 K range. Notably, the Wilson equation successfully corrected for the non-ideal behavior of the Pb-Sb melt ($\gamma_{Pb} \neq 1$), providing more accurate predictions of equilibrium residual lead content, which are consistent with the experimentally observed increase in residual lead with temperature.

Under representative laboratory conditions (1073 K, $H_3PO_4/(NaPO_3)_6$ mass ratio 2:1, composite addition 60 wt.% relative to alloy mass, and a holding time of 10 min), the lead content decreased from 10.00 wt.% to 0.018 wt.%, corresponding to a lead removal efficiency of 99.86%, while maintaining an Sb recovery of 78.7%.

Kinetic analysis indicates that lead removal is primarily controlled by interfacial chemical reactions, with an apparent activation energy of approximately 105 kJ/mol. This is consistent with the experimentally observed temperature dependence of lead removal performance, suggesting that the overall rate in the investigated range is governed mainly by chemical reaction kinetics rather than mass transfer limitations.

The moderate direct Sb recovery (~78.7%) observed under laboratory conditions is mainly associated with Sb volatilization, oxidation, and mechanical entrainment into the phosphate-rich slag. Future improvements may be achieved through enhanced control of the gas atmosphere, optimization of slag composition to reduce viscosity, and shortened high-temperature residence time.

Although the present study is conducted at laboratory scale, the proposed phosphate-based refining route exhibits several features favorable for further scale-up, including a short reaction time and the avoidance of chlorine-based gaseous reagents. From an industrial perspective, key considerations for potential scale-up include reagent consumption, energy input required to maintain the molten state, slag handling, and efficient phase separation. These aspects require systematic evaluation and process optimization in future pilot-scale studies.

Compared with traditional methods, the proposed process achieves a short reaction time (10 min), avoids chlorine-based off-gas and substantially reduces hazardous emissions, and demonstrates potential applicability for further scale-up with appropriate process control. With appropriate gas/slag handling and enhanced interfacial mixing, the approach offers a clean and efficient route for crude antimony refining and may inform impurity removal in other non-ideal alloy systems.

Author Contributions: J.Y. and X.K.: Supervision, D.L.: Project administration, J.T.: Literature search; figure preparation; experimental work; data collection; data analysis; manuscript drafting. X.K.: Study conception and design; data analysis; manuscript review and editing. J.Y.: Study conception and design; data analysis; data interpretation. D.L.: Study conception and design; Resource support; funding acquisition; data interpretation. H.Y.: Study conception and design; Manuscript review and editing; data interpretation; study supervision. All authors have read and agreed to the published version of the manuscript.

Funding: This work was supported by the National Key Research and Development Program of China [Grant No. 2022YFC2904204].

Data Availability Statement: The original contributions presented in this study are included in the article. Further inquiries can be directed to the corresponding author.

Conflicts of Interest: The authors declare no conflict of interest.

References

1. Zhao, T.C. *Antimony*; Metallurgical Industry Press: Beijing, China, 1987.
2. Lei, T.; Zhu, C.J.; Zhang, H.P. *Antimony Metallurgy*; Metallurgical Industry Press: Beijing, China, 2009.
3. Zhou, Y.J. *Forecast of Antimony Demand and Analysis of Supply-Demand Pattern*; China University of Geosciences: Beijing, China, 2015.
4. Anderson, C.G. The metallurgy of antimony. *Geochemistry* **2012**, *72*, 3–8. [CrossRef]
5. Ran, J.-M.; Shi, W.-G.; Zheng, Y.-Q. Study on the Production Process of Refined Lead from Jamesonite. *Hunan Nonferrous Met.* **2004**, *2*, 15–16.
6. Qiu, K.Q.; Dai, Y.N.; Chen, F. Study on Thermodynamic Properties of the Pb-Sb Binary System. *Nonferrous Met.* **1990**, *42*, 49–53.
7. Cai, W.; Xu, B.Q.; Yang, B. Preparation of Titanium Carbide Powder by Vacuum Carbothermal Reduction. *Trans. Nonferrous Met. Soc. China* **2011**, *21*, 185–190.
8. Yuan, H.-B.; Yang, B.; Xu, B.-Q.; Yu, Q.-C.; Feng, Y.-B.; Dai, Y.-N. Aluminum Production by Carbothermo-Chlorination Reduction of Alumina in Vacuum. *Trans. Nonferrous Met. Soc. China* **2010**, *20*, 1505–1510. [CrossRef]
9. Yang, C.Y.; Qiu, K.Q.; Lin, D.Q. Separation of Pb-Pt Alloy by Vacuum Distillation. *Chin. J. Process Eng.* **2009**, *9*, 887–891.
10. Jia, G.B.; Yang, B.; Liu, D.C.; Fan, G. Study on Vacuum Distillation of Waste Pb-Sn Alloy. *Chin. J. Vac. Sci. Technol.* **2006**, *26*, 30–32.
11. Wei, Q.S.; Yang, B.; Li, Y.F.; Liu, H.; Dai, Y.N. Study on Zinc Removal from Waste Aluminum Alloy by Vacuum Distillation. *Chin. J. Vac. Sci. Technol.* **2012**, *32*, 425–429.
12. Li, L.; Liu, D.C.; Yang, B.; Xu, B.Q.; Tang, W.Q. Study on Preparation of Crude Antimony from Lead Anode Slime by Vacuum Distillation. *Chin. J. Vac. Sci. Technol.* **2012**, *32*, 301–305.
13. Du, G.S.; Yang, B.; Dai, Y.N. Study on Removal of Cd, Zn, Tl and Pb from Metallic Materials by Vacuum Distillation. *Yunnan Chem. Technol.* **2006**, *33*, 28–31.
14. Chen, J.J.; Jiang, W.L.; Yang, B.; Liu, D.C.; Dai, Y.N. Study on Separation of Pb-Cu Alloy by Vacuum Distillation. *Chin. J. Vac. Sci. Technol.* **2013**, *33*, 490–495.
15. Jiang, W.L.; Chen, J.J.; Li, Y.F.; Yang, B.; Liu, D.C. Study on vacuum separation of Pb-Ag alloy. *Chin. J. Vac. Sci. Technol.* **2014**, *34*, 18–25.
16. Xu, J.J.; Gao, J.B.; Kong, L.X.; You, Y.J.; Yang, B. Study on Azeotropy and Vapor-Liquid Equilibrium of Pb-Sb Alloy. *Nonferrous Met. (Extr. Metall.)* **2020**, *12*, 5–11.
17. Zhang, F.; Xu, B.Q.; Deng, Y. Research Status and Prospects of Crude Antimony Refining in China. *J. Kunming Univ. Sci. Technol. (Nat. Sci. Ed.)* **2021**, *46*, 1–8.
18. Liu, B.L.; Li, J.M. Ammonium Salt Lead Removal Method for Antimony Pyrometallurgical Refining. Chinese Patent CN1123335A, 29 May 1996.
19. Liu, B.L.; Li, J.M.; Li, R.H. High-Efficiency Lead Removal Method for Antimony Pyrometallurgical Refining and Its Liquid Lead Remover. Chinese Patent CN1127793A, 31 July 1996.
20. Ye, L.G.; Yang, S.H.; Tang, C.B. Application of $NaPO_3$ in Lead Removal During Crude Antimony Pyrometallurgical Refining. *Chin. J. Eng.* **2015**, *37*, 1429–1433.
21. Ye, L.; Hu, Y.; Xia, Z.; Chen, Y. Separation of lead from crude antimony by pyro- refining process with $NaPO_3$ addition. *JOM* **2016**, *68*, 1541–1546. [CrossRef]
22. Zhang, T.; Zhang, X.L.; Wang, B.G. Lead Remover for Antimony Pyrometallurgical Refining and Its Application. CN102041399A, 4 May 2011.
23. Zhang, X.L.; Zhang, T.; Zhang, C. A Lead Remover for Antimony Molten Extraction Refining. CN1455010A, 12 November 2003. pp. 11–12.
24. Barin, I.; Knacke, O.; Kubaschewski, O. *Thermochemical Properties of Inorganic Substances*; Springer: New York, NY, USA, 1972.
25. Wilson, G.M. Vapor-liquid equilibrium. XI: A new expression for the excess free energy of mixing. *J. Am. Chem. Soc.* **1964**, *86*, 127–130. [CrossRef]
26. Silverman, N.; Tassios, D. Prediction of multicomponent vapor-liquid equilibrium with the Wilson equation: Effect of the minimization function and of the quality of binary data. *Ind. Eng. Chem. Process Des. Dev.* **1984**, *23*, 586–589. [CrossRef]

27. Predel, B.; Madelung, O.; Landolt, H. *Phase Equilibria, Crystallographic and Thermodynamic Data of Binary Alloys*; Springer: New York, NY, USA, 1991.
28. Guthrie, R.I.L. *The Physical Properties of Liquid Metals*; Oxford University Press: Oxford, UK, 1988.

Disclaimer/Publisher's Note: The statements, opinions and data contained in all publications are solely those of the individual author(s) and contributor(s) and not of MDPI and/or the editor(s). MDPI and/or the editor(s) disclaim responsibility for any injury to people or property resulting from any ideas, methods, instructions or products referred to in the content.